Supplementary Information for: Conditional probability density functional theory for solids

Peiwei You,[1,*] Ryan Pederson,[2] Kieron Burke,[2,†] and E. K. U. Gross[1,3,‡]

[1] *Fritz Haber Center for Molecular Dynamics, Institute of Chemistry, The Hebrew University of Jerusalem, Jerusalem 91904, Israel*
[2] *Departments of Physics and Astronomy and of Chemistry, University of California, Irvine, California 92697, USA*
[3] *Quantum Dynamics Laboratory, Tsientang Institute of Advanced Study, Hangzhou, Zhejiang, 310024, P.R. China*

This supplementary information contains implementation details of CP-DFT calculations, theoretical background on pair distribution functions, and extensive supplementary data for sodium, helium, Silicon and CsV_3Sb_5 systems.

CONTENTS

This file includes:

- Supplementary Note 1: CP-DFT framework
- Supplementary Note 2: Calculation Methods
- Supplementary Note 3: Pair distribution function
- Supplementary Figures S1-S11

SUPPLEMENTARY NOTE 1: CP-DFT FRAMEWORK

Within the adiabatic connection formalism, we consider an N-electron system subject to a scaled Coulomb repulsion, characterized by a non-negative coupling strength λ, such that the ground-state electronic density $n(\mathbf{r})$ remains fixed [4]. For the λ-dependent N-electron ground-state wave function Ψ^λ, the definition of pair density is written as:

$$P^\lambda(\mathbf{r},\mathbf{r}') = N(N-1)\int dr_3\ldots dr_N \times \left|\Psi^\lambda(\mathbf{r},\mathbf{r}',r_3\ldots r_N)\right|^2 = n(\mathbf{r})\, n^\lambda_{\mathbf{r}}(\mathbf{r}')\,. \tag{1}$$

where $n^\lambda_{\mathbf{r}}(\mathbf{r}')$ is the conditional probability (CP) density: the probability of finding an electron at $\mathbf{r}'$, given an electron at $\mathbf{r}$. Here the spin indices are implicitly summed over. Within second quantization, we can express the pair density as $\langle\Psi|\psi^+(\mathbf{r}')\,\psi^+(\mathbf{r})\psi(\mathbf{r})\psi(\mathbf{r}')|\Psi\rangle$, which constitutes a specific component of the two-particle reduced density matrix.

In Kohn-Sham (KS) density functional theory (DFT), the electronic density $n(\mathbf{r})$ is determined by the KS potential $v_{\rm s}[n](\mathbf{r}') = v[n](\mathbf{r}') + v_{\rm HXC}[n](\mathbf{r}')$ in an N-electrons system. Analogously, in CP-DFT [1, 3], the CP-KS potential for the corresponding $N-1$ electron system with λ-dependent Coulomb repulsion is

$$v^\lambda_{{\rm s},\mathbf{r}}(\mathbf{r}') = v_{\rm s}[n](\mathbf{r}') - v^\lambda_{\rm HXC}[n](\mathbf{r}') + \Delta v^\lambda_{\mathbf{r}}(\mathbf{r}') + v^\lambda_{\rm HXC}[n^\lambda_{\mathbf{r}}](\mathbf{r}')\,, \tag{2}$$

where we have a λ-dependent Hartree exchange-correlation (XC) potentials $v^\lambda_{\rm HXC}$, and $\Delta v^\lambda_{\mathbf{r}}(\mathbf{r}')$ is the CP correction potential [1, 3]. From the CP-KS potential, we establish the λ-dependent CP-KS equation for each reference point $\mathbf{r}$, which is solved self-consistently:

$$\left[T + v^\lambda_{{\rm s},\mathbf{r}}(\mathbf{r}')\right]\phi_{\mathbf{r},i}(\mathbf{r}') = E_{\mathbf{r},i}\phi_{\mathbf{r},i}(\mathbf{r}')\,. \tag{3}$$

where T is the usual kinetic energy operator and $E_{\mathbf{r},i}$ is the eigenvalue and $\phi_{\mathbf{r},i}(\mathbf{r}')$ is the corresponding eigenfunction, where i denotes the index of the eigenfunction. In practical CP-KS calculations, approximations for CP correction potential and XC potential are required. We utilize the local blue electron approximation (LBEA) [1, 3] for the CP correction potential and the Perdew–Burke–Ernzerhof (PBE) [5] XC functional. In the LBEA, the repulsion between

the missing electron at reference point $\mathbf{r}$ and the rest $N-1$ electrons system approaches $\lambda/\left|\mathbf{r}-\mathbf{r}^{'}\right|$ for large separation and goes to $\lambda/(2\left|\mathbf{r}-\mathbf{r}^{'}\right|)$ for small separation to satisfy the electron-electron cusp condition [1–3]:

$$\Delta v_{\mathbf{r}}^{\lambda,\mathrm{LBEA}}\left(\mathbf{r}'\right)=\frac{\lambda}{2\left|\mathbf{r}-\mathbf{r}'\right|}\left[1+\mathrm{Erf}\left(\frac{\left|\mathbf{r}-\mathbf{r}'\right|}{r_{\mathrm{s}}\left(n\left(\mathbf{r}\right)\right)}\right)\right] \tag{4}$$

where r_{s} is the Wigner-Seitz radius.

By employing the uniform coordinate scaling rule, we obtain the λ-dependent energies by the relation $E_{\mathrm{HXC}}^{\lambda}[n](\mathbf{r})=\lambda^2 E_{\mathrm{HXC}}[n_\gamma](\mathbf{r})$, where $\gamma=1/\lambda$ and $n_\gamma(\mathbf{r})=\gamma^3 n(\gamma\mathbf{r})$ [4, 7]. Here n indicates the CP density or KS density. Plugging the coordinate transformation into $\delta E_{\mathrm{XC}}[n_\gamma]$, we establish $\frac{\delta E_{\mathrm{HXC}}[n_\gamma](\mathbf{r})}{\delta n(\mathbf{r})}=v_{\mathrm{HXC}}[n_\gamma](\mathbf{r}/\gamma)$. Thus, the exact potential satisfies:

$$v_{\mathrm{HXC}}^{\lambda}[n](\mathbf{r})=\frac{\delta(\lambda^2 E_{\mathrm{HXC}}[n_\gamma](\mathbf{r}))}{\delta n(\mathbf{r})}=\lambda^2 v_{\mathrm{HXC}}[n_\gamma](\mathbf{r}/\gamma). \tag{5}$$

Since the Hartree-exchange energies are homogeneous scaling, the Hartree and exact exchange potentials simplify to $v_{\mathrm{HX}}^{\lambda}[n](\mathbf{r})=\lambda v_{\mathrm{HX}}\left[n\right](\mathbf{r})$. But correlation energy does not scale as a simple power law. In practice, $v_{\mathrm{C}}\left[n_\gamma\right](\mathbf{r}/\gamma)$ is calculated by transforming $n\to\gamma^3 n, \nabla n\to\gamma^4\nabla n, \int d\mathbf{r}\to\int d(\gamma\cdot\mathbf{r}/\gamma)$, while the conventional unscaled functional is constructed. Then the λ-dependent correlation potential is obtained as $v_{\mathrm{C}}^{\lambda}[n](\mathbf{r})=\lambda^2 v_{\mathrm{C}}[n_\gamma](\mathbf{r}/\gamma)$. Note that some approximate XC functionals may not satisfy the above coordinate scaling conditions in Eq. (5) in general. The PBE [5] functional used in this work satisfies this condition, among others, such as the strongly constrained and appropriately normed (SCAN) functional [6].

After obtaining the KS density, we construct the potential terms of CP-KS equation using the PBE XC functional and LBEA for the CP correction potential $\Delta v_{\mathbf{r}}^{\lambda}\left(\mathbf{r}'\right)$, which requires dense real-space mesh points. The CP-KS equation is solved self-consistently for each reference point $\mathbf{r}$ and each λ, which requires large computational cost but can be easily parallelized. Finally, we obtain the resulting CP density $n_{\mathbf{r}}^{\lambda}(\mathbf{r}')$ on the real-space mesh, and calculate the XC hole by subtracting the KS density from CP density:

$$n_{\mathrm{XC}}^{\lambda}\left(\mathbf{r},\mathbf{r}'\right)=n_{\mathbf{r}}^{\lambda}(\mathbf{r}')-n\left(\mathbf{r}'\right). \tag{6}$$

SUPPLEMENTARY NOTE 2: CALCULATION METHODS

We implement the CP-DFT calculations based on the SIESTA code, utilizing the numerical atomic basis set with double zeta polarization in simulations [8, 9]. The electron-nuclear interactions are described by Troullier-Martins pseudopotentials and standard valence electron configurations are used. The standard KS-DFT are performed firstly to gain the KS density and KS potential. Then, we construct the potential terms of CP-KS equation, adopting the coordinate scaling XC functional and CP correction potential.

For each reference point and each λ (from 0.0 to 1.0, with an interval of 0.25), the CP-KS equation is solved self-consistently when the tolerance of electronic iteration is reached. We remove one electron in the simulation box, by integrating the CP density to $N-1$ electrons in electronic iterations in Eq. (7). The system's net charge is neutralized by the uniform background charge. The PBE is employed throughout the calculations to obtain the λ-dependent XC potential and energy. Distances between each mesh points are directly calculated to obtain the CP correction potential.

All structures are relaxed when the force thresholds are set as 0.01 eV/Å. In all simulations the mixing weight of density matrix is 0.15, and the convergence criterion for the Hamiltonian matrix is set to 1×10^{-4} Ry for self-consistent calculations. For many electrons systems, the gaussian repulsion is added to fix the nonlocality in PBE in terms of CP density, and ensure the CP density is half of KS density at the reference point. The first trial CP density is obtained by scaling the existed KS density with the factor $(N-1)/N$ shown in Eq. (8).

$$\int d\mathbf{r}' n_{\mathbf{r}}^{\lambda}\left(\mathbf{r}'\right)=N-1 \tag{7}$$

$$\text{Initialization: } n_{\mathbf{r}}^{\lambda}\left(\mathbf{r}',\text{trial}\right)=\frac{N-1}{N}n(\mathbf{r}') \tag{8}$$

The lattice constant of Sodium unit cell is 4.22 Å (close to 4.23 Å in experiment [10]), determined by minimizing the total energy with PBE functional. The Brillouin zone is sampled by $6 \times 6 \times 6$ K points, and the energy cutoff is 200 Ry. The energy cutoff is set as 60 Ry to calculate the XC energy.

The single Helium atom is put in the $10\,\text{Å} \times 10\,\text{Å} \times 10\,\text{Å}$ box. The Γ point is used for calculations. An energy cutoff of 500 Ry is used for the plane wave expansion of the charge density. In standard DFT, the radial density and KS potential shown in Fig. S1 are consistent with other reference results beyond the cutoff radius (1 Bohr) of pseudopotential area. In CP-DFT calculations, the cutoff radius of atomic orbitals is 4.7 Bohr, and the energy cutoff of 100 Ry is used to calculate the XC energy.

The lattice constant of Silicon unit cell is 5.48 Å (close to 5.43 Å in experiment), determined by minimizing the total energy with PBE functional. The Brillouin zone is sampled by $10 \times 10 \times 10$ K points, and the energy cutoff is 200 Ry. The energy cutoff is set as 100 Ry to calculate the XC energy. The halfwidth and amplitude of Gaussian repulsion are set to 1.0 and 2.5, respectively.

For Kagome metal CsV_3Sb_5, our routine utilizes optimized unit cell lattice constants of $a = 5.495$ Å and $c = 9.88$ Å by minimizing the total energy with PBE. In the $2 \times 2 \times 1$ ISD phase of CsV_3Sb_5, the deformed Wyckoff sites of V atoms are (0.25318, 0, 0.5) and (0.24630, 0.4926, 0.5) after optimizing the atomic positions. To account for possible long-range electronic orders in the Kagome metal, we expand the cell to a $4 \times 4 \times 1$ supercell, where the Brillouin zone is sampled by $2 \times 2 \times 2$ K points. In the pseudopotentials, 1 valence electrons for Cs atom, 5 valence electrons for V, and 5 valence electrons for Sb are employed. Large real-space mesh grids are necessary, so an energy cutoff of 600 Ry is employed, resulting in a total of 12 million mesh points. The halfwidth and amplitude of gaussian repulsion are set to 0.2 and 6.5, respectively.

SUPPLEMENTARY NOTE 3: PAIR DISTRIBUTION FUNCTION

Within local density approximation (LDA), the XC hole is approximated as a function of electronic density. To obtain the conventional XC hole, we refer to the parametrized LDA of Perdew and Wang (PW92) [11], where the pair distribution function is only related to the relative coordinates $u \equiv \mathbf{r} - \mathbf{r}'$. Once the pair distribution function is obtained, XC hole can be directly calculated via the equation $n_{xc}(u) = n(\mathbf{r})[g(u) - 1]$.

The pair distribution function $g(u)$ is a sum of exchange-only part g_x and correlation part g_c, which are formulated by Eq. (9)-(11). The exchange hole of the homogeneous electron gas is analytically known. The correlation part is parametrized according to quantum Monte Carlo data.

$$g_x = 1 + \frac{1}{2}\left\{(1+\zeta)^2 J\left[(1+\zeta)^{\frac{1}{3}} k_F u\right] + (1-\zeta)^2 J\left[(1-\zeta)^{\frac{1}{3}} k_F u\right]\right\} \tag{9}$$

$$g_c = \left(1 + \frac{r_s \partial}{\partial r_s}\right)\langle \overline{g}_c \rangle \tag{10}$$

$$\langle \overline{g}_c \rangle = \frac{(9\pi/4)^{1/3}}{4/(3\pi)} \phi^3 r_s \frac{\overline{f_1}(v) + \overline{f_2}}{(k_F u)^2} \tag{11}$$

Here $\zeta = (n_\uparrow - n_\downarrow)/n$ is the spin polarization, and $k_F = \left(3\pi^2 n\right)^{\frac{1}{3}}$ is Fermi wave vector. In Eq. (10), $r_s = (3/(4\pi n))^{\frac{1}{3}}$ is Wigner-Seitz radius, and $\langle \overline{g}_c \rangle$ is coupling strength averaged correlation part where $\phi \equiv \frac{(1+\zeta)^{\frac{2}{3}} + (1-\zeta)^{\frac{2}{3}}}{2}$.

The correlation part is a combination of long-ranged ($\overline{f_1}$) and short-ranged part ($\overline{f}_2$) given by Eq. (12)-(13), avoiding the singularity at $u \to 0$:

$$\overline{f_1}(v) = \frac{a_1 + a_2 v + a_3 v^2}{1 + b_1 v + b_2 v^2 + b_3 v^3 + b_4 v^4} \tag{12}$$

$$\overline{f_2} = \left[-a_1 - (a_2 - a_1 b_1)\, v + c_1 v^2 + c_2 v^3 + c_3 v^4 + c_4 v^5\right] e^{-d(\zeta)\left(\frac{k_F u}{\phi}\right)^2} \tag{13}$$

where $v = \phi u \left(\frac{4 k_F}{\pi}\right)^{1/2}$, $d = 0.305 - 0.136\zeta^2$ and other parameters are taken from Ref. [11]. We code these formulas and present the pair distribution function in Fig. S11, showing $g(u)$ is consistent with the data in Ref. [11].

SUPPLEMENTARY FIGURES

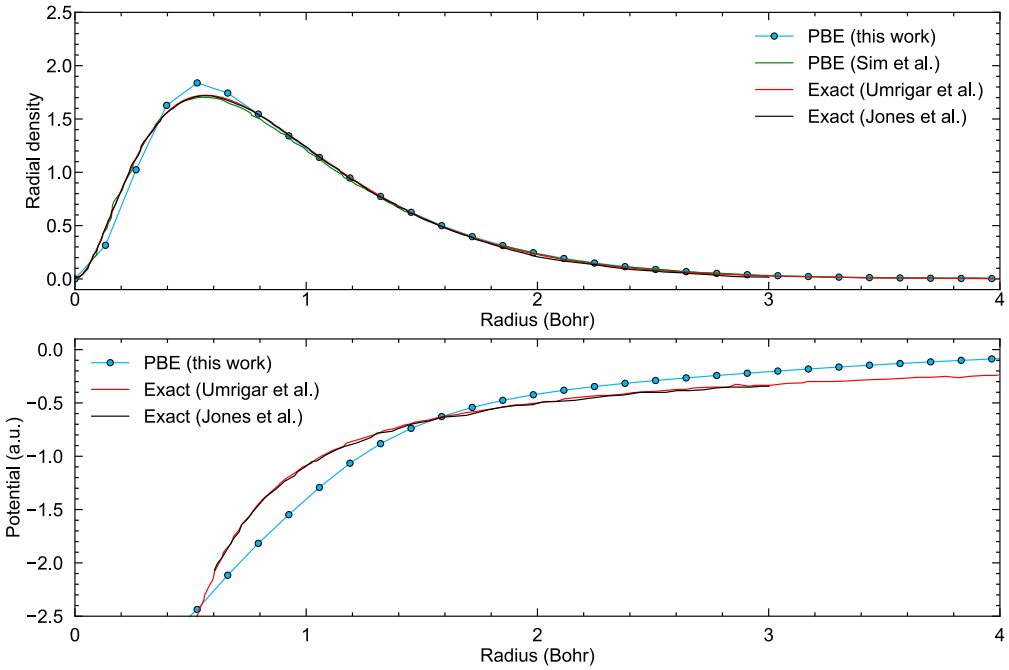

Fig. S1. Radial density and KS potential of one Helium atom with PBE functional. The green, red and black lines indicate the PBE data taken from Sim et al. [12], exact results from Umrigar et al. [13], and exact results from Pribram-Jones et al. [14], respectively.

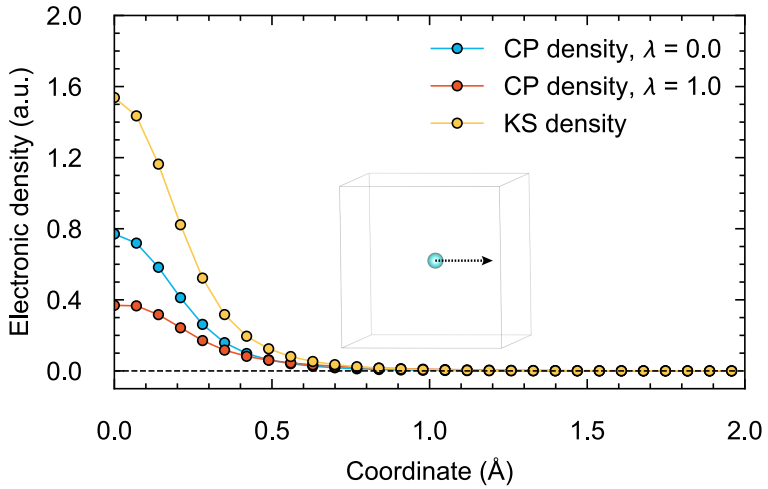

Fig. S2. For the single Helium atom, the CP density linecut with different coupling strengths obtained from CP-DFT and the KS density from KS-DFT, as a function of coordinates from the Helium nucleus. The reference point is at the Helium nucleus. At the reference point, the CP density when $\lambda = 0.0$ is exactly half of KS density.

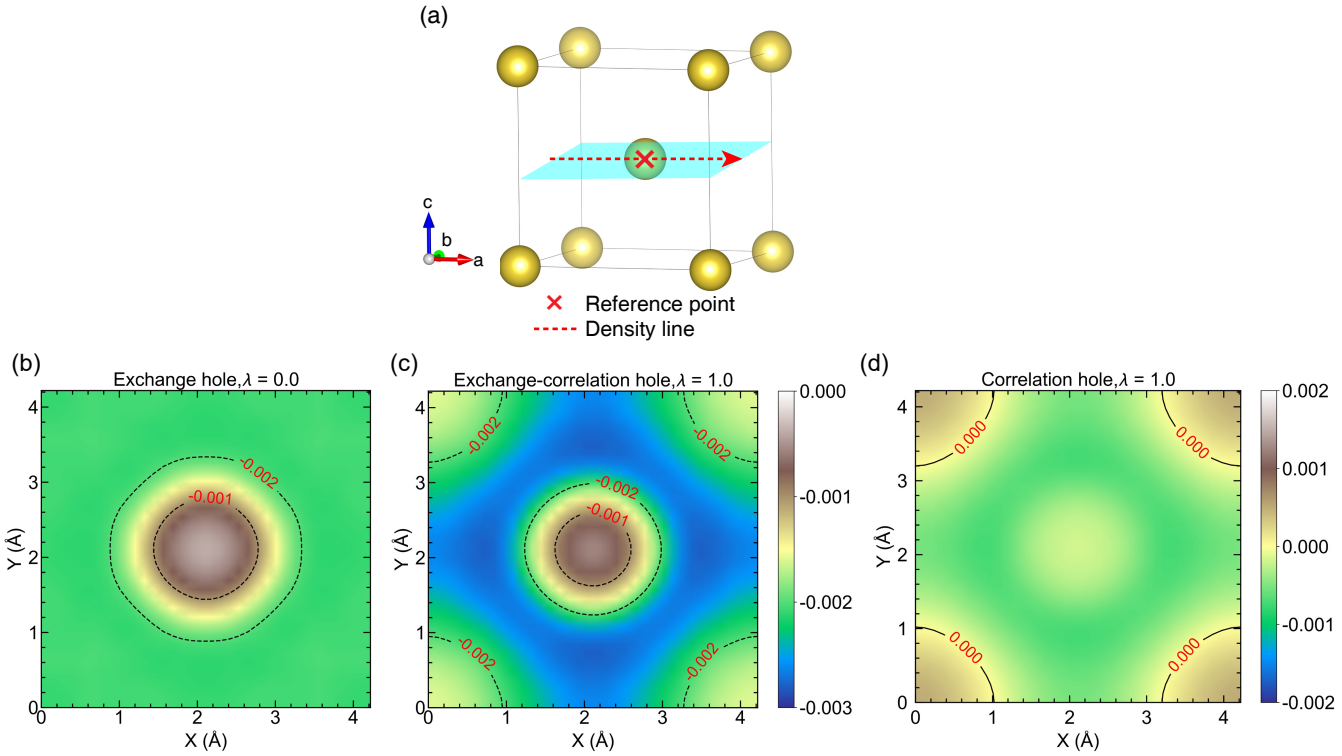

Fig. S3. (a) The atomic structure for the periodic sodium system, where we set the reference point in the center of the box in red cross. The blue surface denotes two-dimensional (001) surface plot at the half of the simulation box. (b-c) Two-dimensional contour plots at the blue two-dimensional (001) surface for the exchange hole ($\lambda = 0.0$) (b) and exchange-correlation hole ($\lambda = 1.0$) (c), by subtracting the KS density from the corresponding CP density. (d) Correlation hole ($\lambda = 1.0$) calculated by using the exchange-correlation hole ($\lambda = 1.0$) to minus the exchange hole ($\lambda = 0.0$). The correlation hole value is scaled by a factor of 5.

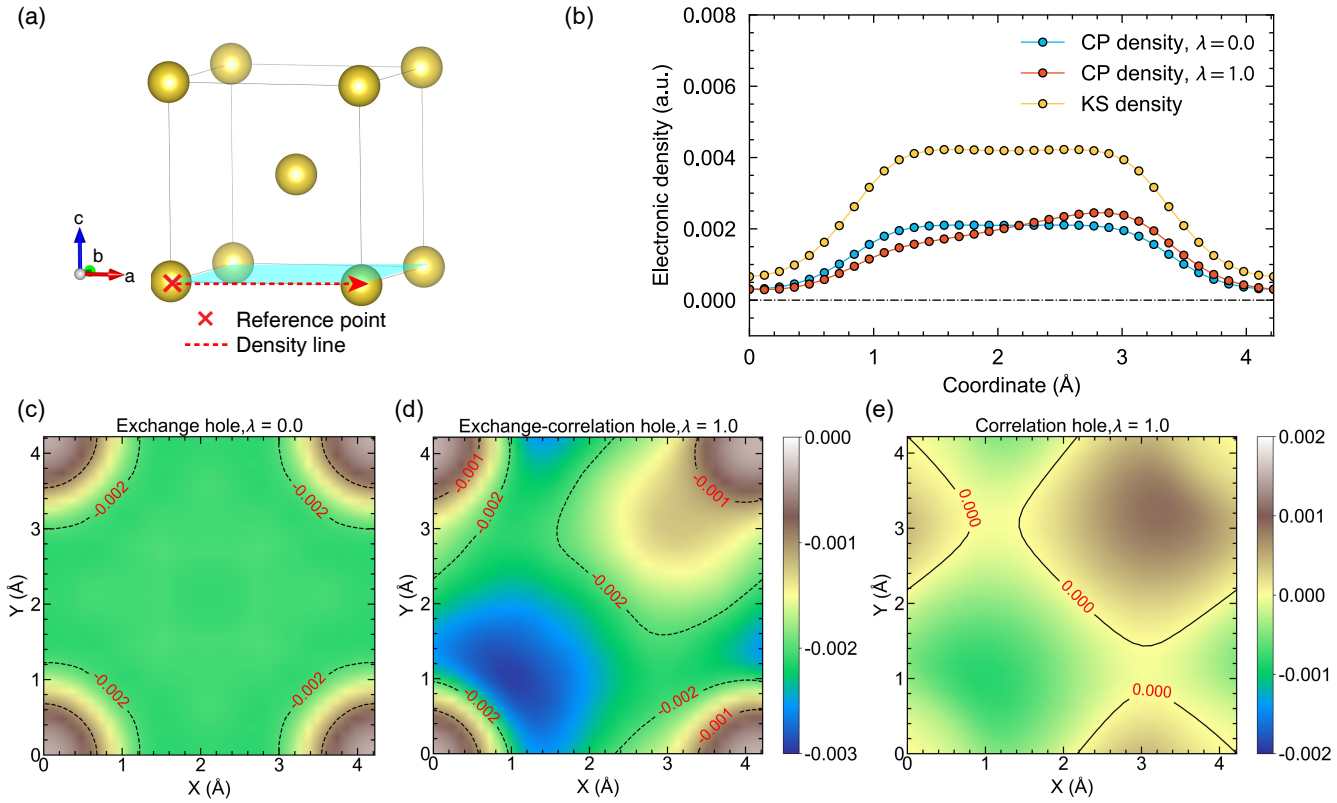

Fig. S4. (a) The atomic structure of Sodium metal. The red cross shows the reference point at the corner. Dashed line and blue surface display density line plot and two-dimensional density plot, respectively. (b) In the Sodium system, the CP density linecut for $\lambda = 0.0$ and $\lambda = 1.0$ obtained from CP-DFT, and the KS density from KS-DFT. The linecut across the original point is denoted in (a) through the blue two-dimensional (001) surface. (c-d) In the blue (001) surface, the exchange hole ($\lambda = 0.0$) in (c) and exchange-correlation hole ($\lambda = 1.0$) in (d), obtained by subtracting the KS density from related CP density. (e) Correlation hole ($\lambda = 1.0$) calculated by using the exchange-correlation hole ($\lambda = 1.0$) to minus the exchange hole ($\lambda = 0.0$). The correlation hole value is scaled by a factor of 5.

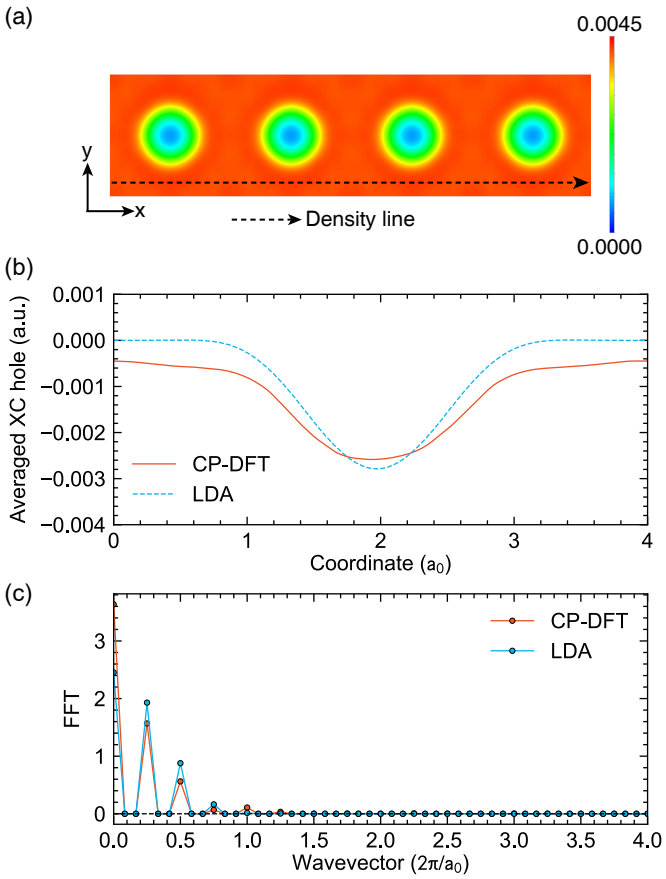

Fig. S5. (a) The two-dimensional KS density at the half surface of the $4 \times 1 \times 1$ Sodium metal. (b) The XC holes from both CP-DFT and LDA along the electronic gas in the supercell, averaged over 18 reference points in 1.5 $a_0 \sim 2.5$ a_0 (with an interval of 0.056 a_0). The density linecut is shown by black arrow in (a). (c) Fourier transform spectrum for the averaged XC hole linecut in (b). Here a_0 denotes the single cell lattice constant of Sodium.

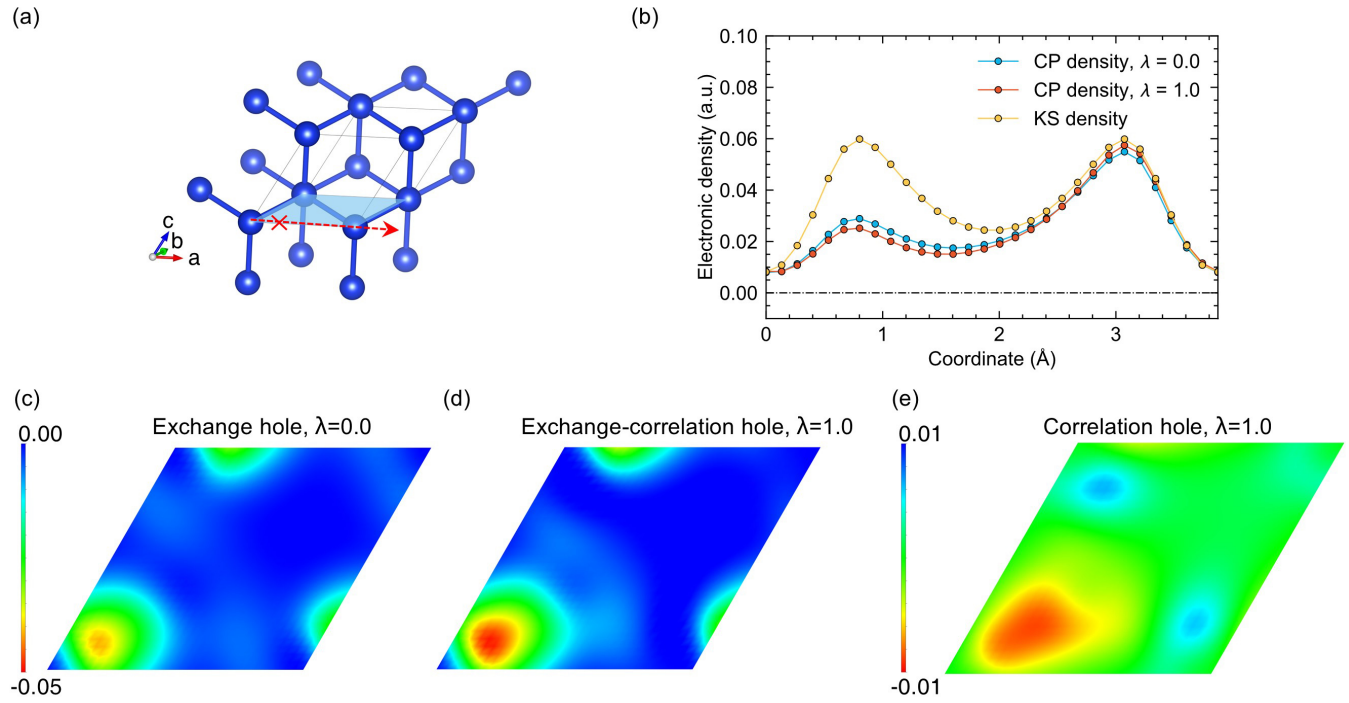

Fig. S6. (a) The atomic structure of bulk Silicon. The red cross shows the reference point located at the KS density peak near the corner. Dashed line and blue surface display density line plot and two-dimensional density plot, respectively. (b) The CP density linecut for $\lambda = 0.0$ and $\lambda = 1.0$ obtained from CP-DFT, and the KS density. The linecut is denoted in (a) through the blue two-dimensional surface. (c-d) In the blue surface, the exchange hole ($\lambda = 0.0$) (c) and exchange-correlation hole ($\lambda = 1.0$) (d). (e) The corresponding correlation hole.

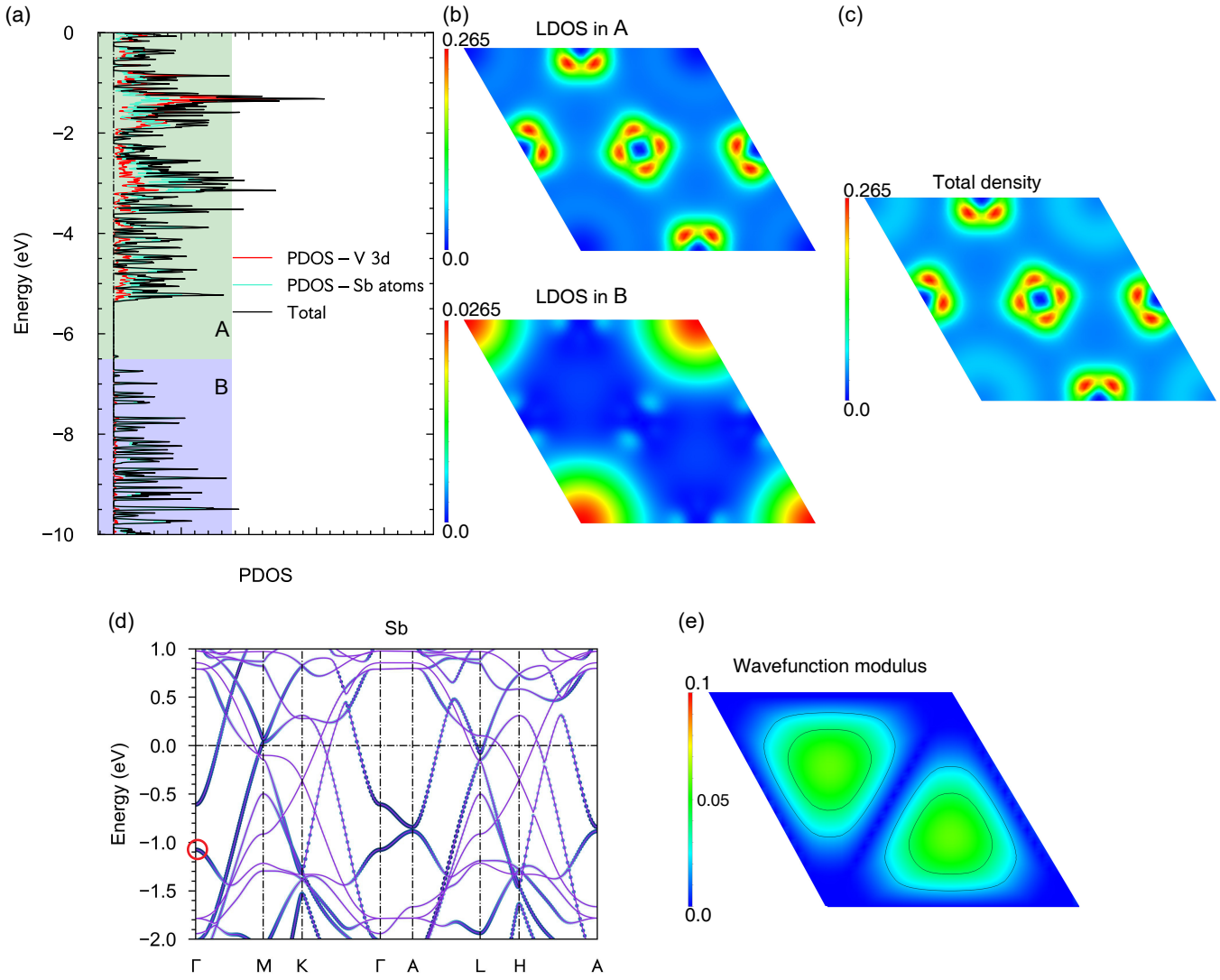

Fig. S7. (a) Projected density of states (PDOS) for V 3*d* and Sb orbitals in the unit cell, with two relevant energy windows marked: A (−6.5 to 0 eV, green) and B (−10 to −6.5 eV, blue). (b) Local density of states (LDOS) mapped in energy windows A (upper) and B (lower). (c) The total electronic density in the unit cell, highlighting distinct "red spot" features. (d) Orbital-resolved band structure for Sb atoms displayed by blue circles. (e) Modulus of a representative wavefunction at the Γ point (−1.1 eV, red circle in (d)), showing an amplitude of ~ 0.02 near the red-spot features of the total density. The red spots in the total density (c) receive no contribution from the deeper energy window B (−10 to −6.5 eV). They originate entirely from window A (−6.5 to 0 eV), which is dominated by 3*d* orbitals. The Sb orbitals contribute negligibly here: their characteristic wavefunction square in this region is < 0.0004 in (e), and other Sb states are oriented out-of-plane. Therefore, the red spots in the total density are predominantly contributed by the V 3*d* orbitals.

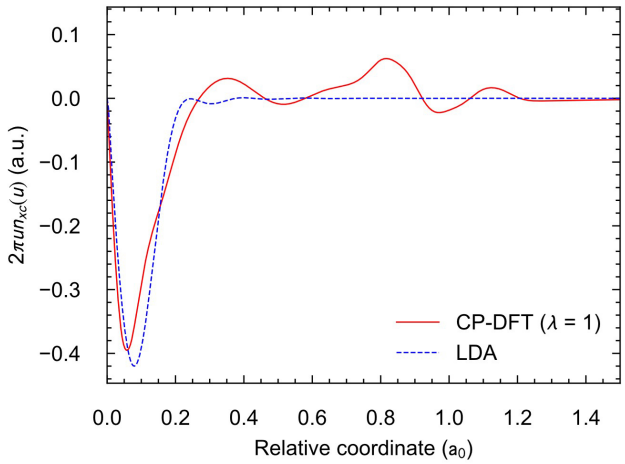

Fig. S8. The scaled XC holes $2\pi u n_{\mathrm{xc}}(u)$ as a function of the relative coordinates $u = \mathbf{r}' - \mathbf{r}$, averaged over 32 reference points in the range of $1.61\,a_0$ to $2.47\,a_0$, and then averaged over both positive and negative values of u.

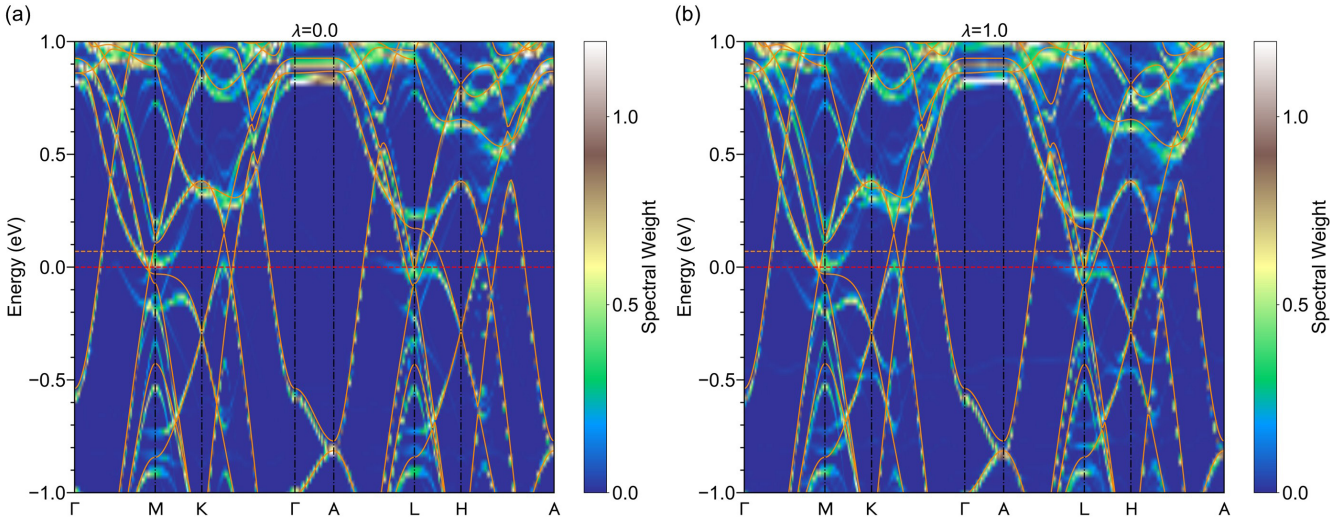

Fig. S9. Unfolded band dispersion of $4 \times 4 \times 1$ supercell with $\lambda = 0.0$ (a) and $\lambda = 1.0$ (b). The orange lines display true band structure of the unit cell. Fermi levels are displayed by dashed red lines for the supercell and dashed orange lines for the unit cell, respectively.

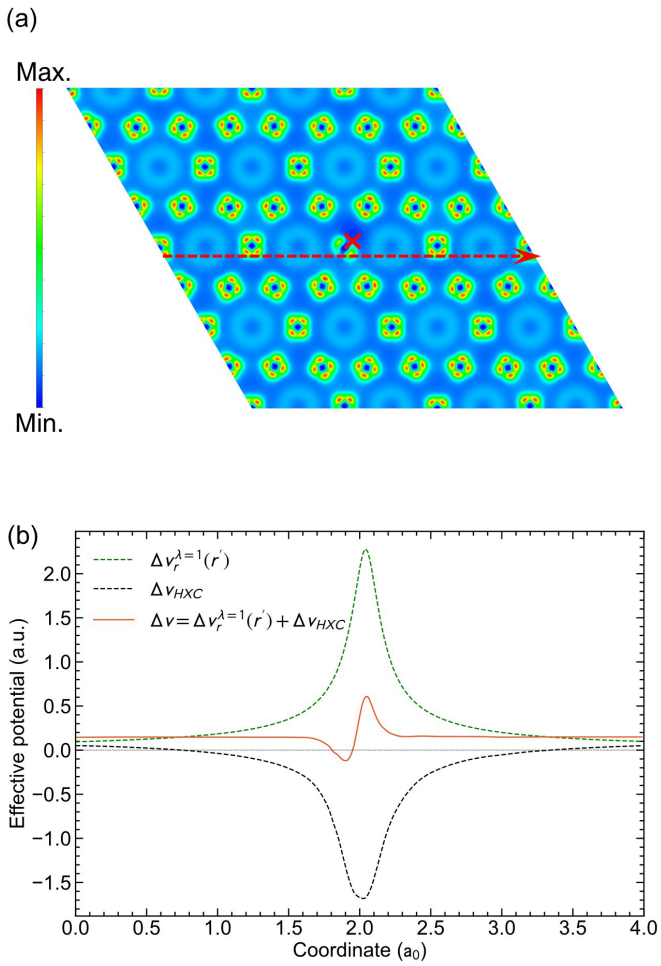

Fig. S10. (a) Two-dimensional CP density distribution with reference points at $x = 2.083\,a_0$, $y = 2.083\,a_0$ denoted by red cross. (b) Comparison of potential differences where the linecut at $y = 1.88\ a_0$ is shown in (a). The green line represents the CP correction potential $\Delta v_{\mathbf{r}}^{\lambda=1}(\mathbf{r}')$, the black line shows the difference of Hartree-XC potential $\Delta v_{\mathrm{HXC}} = v_{\mathrm{HXC}}^{\lambda=1}[n_{\mathbf{r}}^{\lambda=1}](\mathbf{r}') - v_{\mathrm{HXC}}^{\lambda=1}[n](\mathbf{r}')$, and the red line denotes the total difference.

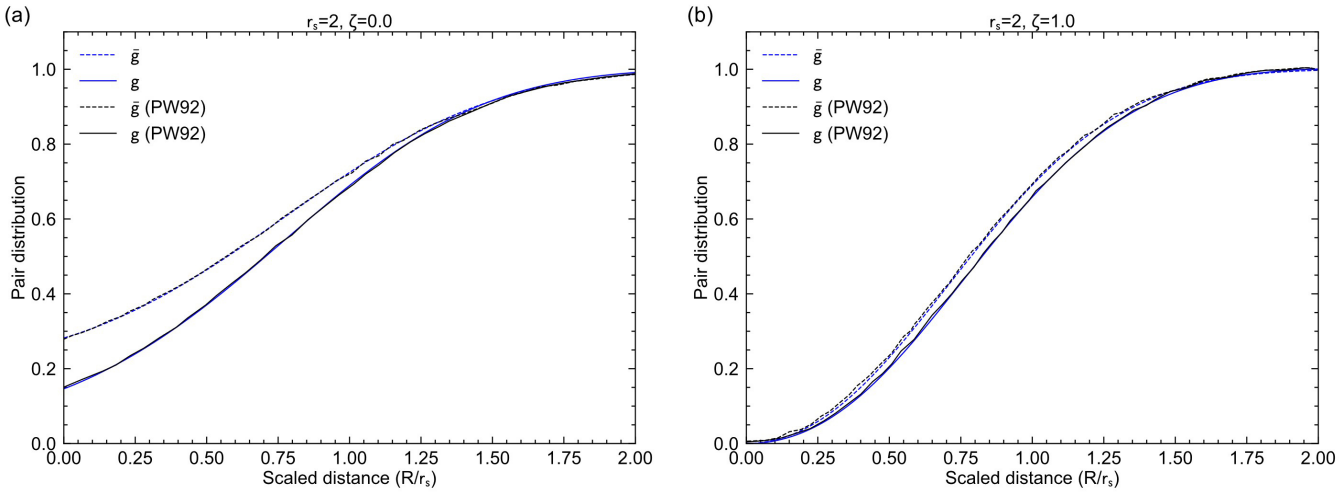

Fig. S11. The total pair distribution function $g(u)$ and coupling constant averaged pair distribution function $\overline{g}(u)$ with different parameters ($r_s = 2$, $\zeta = 0.0$) in (a) and parameters ($r_s = 2$, $\zeta = 1.0$) in (b). Here r_s is Wigner-Seitz radius and $\zeta = (n_\uparrow - n_\downarrow)/n$ is the spin polarization. The Hartree atomic unit is used here. Original PW92 data is scratched from the Ref. [11], displayed by black lines.

REFERENCES

* peiwei.you@mail.huji.ac.il
† kieron@uci.edu
‡ eberhard.gross@mail.huji.ac.il

[1] R. Pederson, J. Chen, S.R. White, K. Burke, Conditional probability density functional theory, Phys. Rev. B **105**, 245138 (2022).
[2] T. Kato, On the eigenfunctions of many-particle systems in quantum mechanics, Commun. Pure Appl. Math. **10**, 151–177 (1957).
[3] R.J. McCarty, D. Perchak, R. Pederson, R. Evans, Y. Qiu, S.R. White, K. Burke, Bypassing the Energy Functional in Density Functional Theory: Direct Calculation of Electronic Energies from Conditional Probability Densities, Phys. Rev. Lett. **125**, 266401 (2020).
[4] C. Fiolhais, F. Nogueira, M.A.L. Marques, A primer in density functional theory (Springer Science & Business Media, 2003).
[5] J.P. Perdew, K. Burke, M. Ernzerhof, Generalized gradient approximation made simple, Phys. Rev. Lett. **77**, 3865–3868 (1996).
[6] J. Sun, A. Ruzsinszky, J.P. Perdew, Strongly Constrained and Appropriately Normed Semilocal Density Functional, Phys. Rev. Lett. **115**, 036402 (2015).
[7] A. Görling, M. Levy, Correlation-energy functional and its high-density limit obtained from a coupling-constant perturbation expansion, Phys. Rev. B **47**, 13105–13113 (1993).
[8] J.M. Soler, E. Artacho, J.D. Gale, A. García, J. Junquera, P. Ordejón, D. Sánchez-Portal, The SIESTA method for ab initio order-N materials simulation, J. Phys.: Condens. Matter **14**, 2745–2779 (2002).
[9] A. Garcia, N. Papior, A. Akhtar, E. Artacho, V. Blum, E. Bosoni, P. Brandimarte, M. Brandbyge, J.I. Cerda, F. Corsetti, R. Cuadrado, V. Dikan, J. Ferrer, J. Gale, P. Garcia-Fernandez, V.M. Garcia-Suarez, S. Garcia, G. Huhs, S. Illera, R. Korytar, P. Koval, I. Lebedeva, L. Lin, P. Lopez-Tarifa, S.G. Mayo, S. Mohr, P. Ordejon, A. Postnikov, Y. Pouillon, M. Pruneda, R. Robles, D. Sanchez-Portal, J.M. Soler, R. Ullah, V.W. Yu, J. Junquera, Siesta: Recent developments and applications, J. Chem. Phys. **152**, 204108 (2020).
[10] C. Kittel, P. McEuen, Introduction to solid state physics (John Wiley & Sons, 1986).
[11] J.P. Perdew, Y. Wang, Pair-distribution function and its coupling-constant average for the spin-polarized electron gas, Phys. Rev. B **46**, 12947 (1992).
[12] M.C. Kim, E. Sim, K. Burke, Understanding and reducing errors in density functional calculations, Phys. Rev. Lett. **111**, 073003 (2013).
[13] C.J. Umrigar, X. Gonze, Accurate exchange-correlation potentials and total-energy components for the helium isoelectronic series, Phys. Rev. A **50**, 3827 (1994).
[14] A. Pribram-Jones, D.A. Gross, K. Burke, DFT: A Theory Full of Holes?, Annu. Rev. Phys. Chem. **66**, 283 (2015).